47th AIAA Aerospace Sciences Meeting Including The New Horizons Forum and Aerospace Exposition
5 - 8 January 2009, Orlando, Florida

AIAA 2009-679

47th AIAA Aerospace Sciences Meeting and Exhibit
5 - 8 January 2009, Orlando, Florida

AIAA-2009-0679

Active Cooling of Turbine Blades using Horse-Shoe Plasma Actuator

Chin-Cheng Wang* and Subrata Roy§
Computational Plasma Dynamics and Test Facility
Mechanical and Aerospace Engineering Department
University of Florida, Gainesville, FL 32611-6300

We numerically test two novel concepts for film cooling enhancement in gas turbines and other engineering applications. The first concept utilizes electric force to induce attachment of cold jet to the work surface by actively altering the body force in the vicinity using a horse-shoe shaped plasma actuator. Two different force models have been utilized: (1) spatially distributed electric force based on phenomenological model, and (2) time averaged reduced order model. For the other concept, we propose three geometric modifications of the cooling hole exit for enhancing lateral tripping of the cold jet. We have shown that a combination of plasma and geometric change can significantly improve the film cooling performance. Numerical predictions with finite volume based simulation are performed using standard turbulence models. Detailed computation of a single row of 35 degree round holes on a flat plate has been obtained for a unit blowing ratio. Results are compared with the published experimental data and other numerical predictions for the latest film cooling technology to identify effectiveness improvement. The numerical results show an improvement of effectiveness well above 100% over the standard baseline design.

Nomenclature

C_1 - C_6	=	force constant
D	=	major axis of cooling hole exit conical section (mm)
d	=	circular pipe diameter (mm)
F	=	actuation body force density (N/m^3)
L	=	distance between hole centers (mm)
M	=	blowing ratio, $\rho_j u_j/\rho_f u_f$
P_f	=	freestream inlet pressure (Pa)
r	=	radius, $(x^2 + y^2)^{0.5}$ (m)
T	=	local static temperature (K)
T_{fs}	=	freestream gas temperature (K)
T_j	=	cooling jet temperature (K)
T_s	=	work surface temperature (K)
u_{fs}	=	freestream velocity (m/s)
u_j	=	jet velocity at exit plane (m/s)
u	=	x-component of the velocity (m/s)
v	=	y-component of the velocity (m/s)
α	=	jet issuing angle
β	=	function of the dielectric material
ϕ	=	potential (volts)
η	=	film cooling effectiveness, $(T_{fs}-T_s)/(T_{fs}-T_j)$
Λ	=	amplitude of actuation force density (kN/m^3)
ρ_{fs}	=	freestream gas density (kg/m^3)
ρ_j	=	cooling jet density (kg/m^3)

* Graduate Student, Student Member AIAA, james614@ufl.edu
§ Associate Professor, Associate Fellow AIAA, roy@ufl.edu

I. Introduction

Active cooling of hot surfaces with cold fluid film is of critical need for many engineering problems. One such application of interest is gas turbine blades. Gas turbines blades suffers from very high thermal stresses due to hot effluent gases from the combustor. The problem worsens with higher turbine inlet temperature need for generating more power. Repetitive stress over a long duration significantly affects the lifetime of turbine blades. A method for reducing such thermal stress and thus for increasing lifetime for a turbine blade is to inject cold jets through a row of surface holes located in the spanwise direction. The resultant penetration of the cold jet into the hot mainstream flow creates a three-dimensional flow field. Such method is known in the industry as film cooling. The trajectory and physical path of thermal jet and the mixing mechanism of jet in the crossflow are critical design parameters. For our study we specifically choose flat plate (not curved blade) geometry to make it suitable for general application. Figure 1 shows the schematic of a single round jet injected in the crossflow at an angle. This geometry has been extensively investigated for cooling performance for a wide range of blowing ratio (i.e., momentum ratio of injected air to crossflow).

A summary of basic investigations of isothermal and thermal jets into crossflow is given in our prior publication[1,2]. These results show details of the vortex interaction region, and mixing and mean centerline species concentration decay in the near and far field. Despite various innovative techniques[3,4], the film cooling effectiveness is ultimately limited by the loss of flow attachment just downstream of the hole. This is due to the "lift-off" of the cold jet beyond a threshold momentum ratio. The film cooling configuration which is designed for peak flow performance may not actively regulate itself for off-design conditions. As a viable alternative, in this paper we present two possible novel designs of film cooling flow for the three-dimensional geometry shown in Figure 1. We explore ways to actively enhance interaction of cool air jets with hot crossflow for improved cooling of hot surfaces.

An important parameter for comparing film cooling performance is its effectiveness $\eta = (T_{fs} - T_s)/(T_{fs} - T_j)$, where T_s, T_j and T_{fs} are the work surface, cooling jet and freestream gas temperatures, respectively. The effectiveness is plotted against a non-dimensional ratio x/Md, where x is the downstream distance, $M = \rho_j u_j/\rho_{fs} u_{fs}$ is the blowing ratio, and d is the circular pipe diameter. The density ρ_j and velocity u_j of the fluid at the jet exit plane are related to the freestream density ρ_{fs} and velocity u_{fs} such that $\rho_j/\rho_{fs} = M u_{fs}/u_j$. As compared to the slots, a row of discrete holes typically has a much lower span averaged downstream film effectiveness distribution for the same x/Md ($=x/d$ for $M=1$) due to the formation of vortices which allow hot gas to penetrate to the wall. These vortices are of the scale of the hole size and smaller. It is essential for a computational mesh to have a minimum node spacing much smaller than the film hole spanwise pitch. Otherwise, such calculation becomes two-dimensional on the scale of the film holes. Several experimental efforts[4-6] have been documented in the literature. They measured the scaling effect of the hole spacing to diameter ratio and the influence of the inclination of the holes to the surface on a flat plate and on curved (turbine blade-like) surfaces at different flow thermal conditions. Bunker[7] also provided a review of the shaped holes for film cooling. He summarized the benefits of shaped hole such as higher centerline and spanwise effectiveness than round hole and little variation in effectiveness over blowing ratio from 0.5 to 2.

Numerical solutions of the full Navier-Stokes equations have also been used to obtain detailed solutions in various studies[1,2,8-12]. These efforts include closure models based on constant turbulent viscosity, variants of Reynolds averaged Navier-Stokes (RaNS), large eddy simulation (LES) and hybrid turbulence models (like DES). Numerical solutions for these flow arrangements document strong to moderate secondary vortex structures spanning normal to the direction of the jet. This fully three-dimensional flow field strongly influences the cooling performance of the hole-blade system. Computational results predict an optimum hole spacing and low issuing angle for maximum cooling efficiency[1].

Several computational studies have computed turbine blade geometries with accurate resolution of the cooling holes, and in some cases, of the hole pipes and plena as well. Garg and Rigby[10] resolved the plenum and hole pipes for a three-row showerhead film cooling arrangement with Wilcox's k-ω turbulence model, and Heidmann *et al.*[11] used Reynolds-averaged Navier–Stokes (RaNS) to compute the heat transfer for a realistic turbine vane with 12 rows of film cooling holes with shaped holes and plena resolved. Garg[12] presented results of a full rotating blade with 172 film holes, resolving the cooling hole exits, but not the hole pipes and plenum. These studies provide good details of the flow. However, the anisotropic dynamic nature of the spanwise vortices that affect the film cooling

process are more complex than that can be captured by the mixing models used in aforementioned papers. The two competing factors important for any turbulence model are accuracy and efficiency (i.e. computational cost). An optimal combination of both these factors is hard to achieve and thus, the primary purpose of the numerical simulation is towards attaining such a goal. Although, LES requires less computational effort or can simulate flows at higher Reynolds number than direct numerical simulation (DNS), one major challenge for performing LES in film cooling is the range of length scales that must be resolved in the computation (Lesieur *et al.*[13]). As a remedy, Kapadia *et al.*[2] utilized a detached eddy simulation (DES) turbulence model[14] on a widely published blade-pipe configuration for a unit blowing ratio. DES model makes no such assumption of isotropy downstream of the hole. Results indicate that the mixing processes downstream of the hole are highly anisotropic, as the turbulent diffusion is much stronger in the transverse direction. In comparison to the RaNS solution temperature distribution on the blade and near the vertical symmetry plane, DES captured better description of the dynamic flow structures.

In the near field of the film cooling jet, the dynamic large scale structures control the mixing process[2,15]. This three-dimensional mixing shown in Figure 2 determines the normal and transverse penetration of the jet. We conjecture that accurate actuation of such flow field will greatly influence the near wall heat transfer process and the film cooling effectiveness. The complex dynamic nature of the spanwise vortices makes it necessary to use active mode of control that will interact with the flow field temporally and spatially in the near wall region. We will utilize the surface region for actively controlling the coolant flow and its three-dimensional spread over the work surface.

We introduce the following two new concepts as described in Figure 3. Let us consider the first configuration shown in Figure 3(A). Here we use horse-shoe plasma actuator (Roy and Wang[16]) at the downstream (or upstream) of the cooling hole. Such actuators are made of a set of electrode pairs between which electric potential and induced weak ionization of the working gas generate an electric body force that is dominant inside the boundary layer. In such an actuator the flow actuation is directly linked with the gas-charged particle interaction and thus instantaneous. A small fraction of power (less than 1% of the turbine power) will be utilized for such arrangement which may eventually reduce the energy budget by more effective cooling.

The second concept is to utilize alternate designs of the cooling hole exit. Figure 3(B) shows schematics of various shapes of the hole exit plane: (a) baseline; (b) bumper with 0.5*d* height; (c) jet hole with compound slopes, (d) rectangular slot. The intension of the shapes (c) and (d) is to trip the emerging cold jet. The purpose of all these geometries is to reduce the lift-off effect of the cold jet by a tripping mechanism, so that it attaches to the surface downstream of the hole. The bumper is introduced to trip the cold flow in a direct fashion. Such configurations may be used in conjunction with the plasma actuation described above.

II. Electric Force Model

The complex dynamic nature of the film cooling flow makes it necessary to actively control it with a dynamic force that varies temporally and spatially working with the dominant turbulence scales. Both pulsed dc and ac powered plasma actuators can induce such active control over the dynamics of film cooling.

The induced force in such actuators is local (within a few mm) and diminishes quickly outside the domain of influence as shown in Figure 4 schematic below. The actuator can be of the form as shown in Figure 3(A) where the powered and grounded electrodes are kept at a sequence to push the fluid in the forward direction. A dc or ac voltage of several hundreds of volts may be applied to the powered electrode costing a few hundred watts per meter of the turbine blade. Such configurations are based on documented numerical experience and experimental evidence[17-19]. The momentum transfer between the plasma and gas happens due to collisional momentum transfer between charged ions and neutral atoms. High freestream gas temperature will enhance dissociation and hence help plasma generation due to ionization in the vicinity of the electrodes. Such actuation of the flow is active and near instantaneous, does not require any mechanical parts, and the actuator electrode sets can be applied as a patch on the surface of the existing ceramic coating of the turbine blade or embedded into the coating. There could be practical considerations like surface oxidation of the electrodes and spallation. These need to be investigated during in situ testing and out of the scope for the present paper. We presented two different approaches to model the physics of plasma actuators. The first approach is the phenomenological model, which is based on force distribution approximation. The second approach is the reduced order model which correlates the relationship among the force, the load parameters (voltage and frequency), and the geometric parameters. The approximated force is an

exponentially decaying distribution with its peak just downstream of the cooling hole exit. While in practical situation this force will be transient, we consider the time average of the electric force as a local body force term in our simulation. This is allowable due to largely disparate timescales of plasma and gas flow.

For the phenomenological model, the actuator force density is represented by $F = +6F\hat{i} - 3F\hat{j} \pm F\hat{k}$ shown in Figure 5(A), where $F = \Lambda * f_x * f_y * f_z$, Λ is amplitude, $f_x = [(x\text{-}d/2)^2\text{-}C_1]/C_2$, $f_y = [(y\text{-}d/2)^2\text{-}C_3]/C_4$, $f_z = [\exp(-1000z)/C_5)]\text{-}C_6$. The amplitude Λ is varied from 0 to 7500 kN/m^3 with an increment of 1500 kN/m^3 and $C_1 = 1.5\times10^{-6}$, $C_2 = 3.09\times10^{-6}$, $C_3 = 1.58\times10^{-6}$, $C_4 = 3.14\times10^{-6}$, $C_5 = 0.98$, $C_6 = 0.057$. For the reduced order model, we used the modified force model from Singh and Roy[20]. The modified form: $F = \Lambda * F_{x0} * \phi_0^4 * \exp[-((r\text{-}r_0)\text{-}(z\text{-}z_0))/z)^2\text{-}\beta_x (z\text{-}z_0)^2]\hat{i}$ $+\Lambda * F_{y0} * \phi_0^4 * \exp[-((r\text{-}r_0)\text{-}(z\text{-}z_0))/z)^2\text{-}\beta_y (z\text{-}z_0)^2]\hat{j} + \Lambda * F_{z0} * \phi_0^4 * \exp[-((r\text{-}r_0)/z)^2\text{-}\beta_z (z\text{-}z_0)^2]\hat{k}$ shown in Figure 5(B), where F_{x0}, F_{y0}, and F_{z0} are taken from the average electrodynamic force obtained by the solving air-plasma equations. The functional relationship with the fourth power of potential $\phi_0 = 800$ V to the exposed electrode is based on the plasma simulation. The values of β_x, β_y, and β_z are functions of the dielectric material and correlated to match the velocity induced by the electrodynamic force.

III. Numerical Method

A. Boundary Conditions

Figure 1 describes schematic control volume of freestream air passing over a flat surface (e.g., a turbine blade). This surface of study has a row of injection holes through which the cool air is issued at an angle $\alpha = 35°$. The cool jet at temperature $T_j = 150$K is injected into the hot freestream of $T_{fs} = 300$K. The injection ducts are circular pipes with diameter equal to $d = 2.54$mm. The injection hole formed by the intersection of the injection pipe with the wind tunnel is an ellipse with the minor and the major axes d and $D = d/(\sin\alpha)$, respectively. The distance between the hole centers is $L = 3d$. The selected mean flow velocities, static pressures and temperatures (i.e., densities) in the injection pipe and the wind tunnel gives a blowing ratio $M = 1$. The inlet section is located at $x = -20d$ and the exit at $x = 29d$. The other dimensions and boundary conditions are shown in Figure 1. The flat (blade) surface is considered adiabatic.

At the freestream inlet $x = -20d$, an injected mass flow rate inlet condition was applied with the density ratio of $\rho_j/\rho_{fs} = 2$, velocity ratio of $u_j/u_{fs} = 0.5$, and turbulent intensity of 5%. At the exit plane $x = 29d$, the gauge pressure at the outlet boundary is maintained at 0 Pa. The work surface is an adiabatic wall with a single row of holes through which cool air at temperature is equal to $T_j = 150$K is injected at an angle of $\alpha = 35°$ into the freestream temperature $T_{fs} = 300$K. The domain extends from the plenum base at $z = -6d$ to $z = 20d$ from work surface where a pressure-far-field boundary condition was applied. The periodic boundary condition was applied in the crosswise direction (at $y = \pm1.5d$) in the computational domain. For the coolant plenum, we applied no-slip wall condition on $x/d = -14$ and 8, and $z/d = -2$ surfaces; mass flow inlet condition for $z/d = -6$; periodic boundary condition on $y/d =$ -1.5 and 1.5.

At the walls, an adiabatic wall boundary condition with no-slip was imposed. For both concept one and two, we impose the time averaged force density shown in Figure 5 based on the phenomenological model and reduced order model. Depending on the actuation device a local kN/m^3 force density may be obtained with a few input watts[21]. For this problem that may require kW level power be applied per meter length of the actuator.

B. Grid information and computational approach

The established 3-D mathematical model was solved by a commercial CFD package, FLUENT 6.3.26, is based on the finite volume method. According to the experiments, it is assumed that the flow is compressible and steady-state turbulent flow. The Reynolds number based on hole diameter and inlet conditions was 16100. A maximum Mach number not exceeding 0.3 was achieved in the flow field while maintaining the desired Reynolds number by scaling the experimental geometry down by a factor of 5. This resulted in a hole diameter of 2.54 mm, and was done to allow more rapid convergence of the solution using the density-based formulation of the computer code while minimizing compressibility effects.

We use the ideal gas approximation and the Advection Upstream Splitting Method (AUSM) solver closed with ReNormalized Group (RNG) k-ε turbulence model with standard wall function[21]. We have also tried the non-equilibrium wall function which resulted in very similar result. The courant number was set equal to 1 for solution control. A second-order upwind discretization method is used. Convergence is determined when the residual among the continuity, momentum, energy, turbulent kinetic energy, and turbulent dissipation are less than 10^{-3}. Figure 6(A) shows the density of computational grid near the coolant hole. When necessary the electic force from Section II was used as a time-averaged body force. The simulation of concept one and two are performed on a mesh around 200000 cells based on the grid independent test for less computational cost. The baseline case takes 1300 iterations for convergence. The baseline solutions are compared with experimental data and are determined to be quite similar. All cases with body force took around 2000 iterations for concept one and around 5500 iterations for concept two.

IV. Results and Discussion

Seventeen cases were simulated for this paper. The cases are one baseline case, ten cases with body force related to concept one, three cases of geometry modifications (concept two), and three combinations of electric body force with geometry modifications. Since we used an inherently time averaged turbulence model, computed results were presented at the steady state. In Figure 6(B), representative velocity vectors colored by speed inside the injection pipe describe the stratification of kinetic energy inside the tube. At steady state, the numerical solution shows that majority fluid is impinging at a high velocity (about 114 m/s) on the upper half of the tube. Near the bottom, the fluid is creating a large recirculation stretching towards the middle of the pipe. As a result at the exit plane of the tube the flow is highly non-uniform. This is in agreement with the qualitative results reported in the literature[2, 22]. Clearly, for this moderate blowing ratio $M = 1$ and a combination of flow profiles at the wind tunnel and cold jet inlet, the effect of the vorticity in the pipe is not negligible. This is due to the fact that at this range of velocities existing in the pipe, the boundary layers are not thin everywhere in the pipe. It is well known that coarse grids cannot resolve the effect of the downstream vortices.

Corresponding flow field stream trace on the velocity magnitude contour in the spanwise direction as shown in Figure 7 at $x = 5d$ shows the well-known kidney shape and the horse-shoe bound vortical structure. The effect of the wind tunnel vorticity is significant at this plane. This is more pronounced in the u and v velocity profiles. The assumption of uniform velocity profile in the wind tunnel leads to higher v values in the near-wall jet flow region. In this case, the maximum in the u velocity is located below the maximum in the case of developed inlet profile in the wind tunnel. The tendency is that as the boundary layer in the wind tunnel becomes thicker, the velocity maxima appear at higher distances from the wall and the near-wall flow changes dramatically. At very thick boundary layers, the flow close to the wall behaves as a typical boundary layer, while for very thin incoming boundary layers a wall-jet flow exists downstream the jet exit. Such flow motion creates a bound kidney shaped vortical structure that stretches downstream along the primary flow direction. Details of such structure are available in our previous publication[1,2].

A. Concept_One

Figures 8-11 describe the effect of the imposed (plasma actuator) body force density on film cooling for both approaches. Figure 8(A) plots the temperature distribution on the vertical mid-plane ($y = 0$) based on phenomenological model. It is obvious that the lift-off effect causes a significant reduction in effectiveness for the baseline case (i). As we increase the body force density from an initial zero ($\Lambda = 0$, no force) to a maximum of $\Lambda = 7500$ kN/m^3 (effective force ~N) the flow completely attaches to work surface. Note that the results based on the reduced order model in Figure 8(B) show less cold jet penetration into the hot gas along the streamwise direction than the phenomenological model. This is also supported by lateral diffusion of the cold jet in the latter case as shown in the following figure.

Figure 9 shows the temperature distribution on the horizontal work surface ($z = 0$) for both approaches. Importantly, the actuation force applied in a three-dimensional manner demonstrates successful spreading of the cold film over the flat (blade) surface not only in the streamwise direction but also in the crosswise fashion. Figure 9(A) plots the prediction based on phenomenology and Figure 9(B) shows first-principles based reduced order

predictions. As the force density increase from Λ = 0 to 7500 kN/m^3, the cold flow attachment has significant effect near the coolant hole. Especially for the reduced order model shown in Figure 9(B), the cooling performance has significant improvement in the crosswise direction due to the larger force density at spanwise directions than the phenomenological model.

Figure 10 plots the centerline effectiveness and the spanwise averaged effectiveness using phenomenological model over the work surface. The computed centerline results for the baseline case (no force) compares reasonably with the experiment of Sinha *et al.*[6] and two other previously reported numerical results[23-24]. We can see the centerline effectiveness decreases for the baseline case as the distance of downstream (x/d) increases due to the lift-off effect. At x/d = 5, the effect of plasma actuation is evident. The centerline effectiveness in Figure 10(A) increases by over 100% as the force density increases to the maximum. The spanwise averaged effectiveness shown in Figure 10(B) also improves demonstrating the three dimensional flow control.

Figure 11 shows the centerline effectiveness based on reduced order model. We can see the cooling performance increases significantly near the coolant hole before x/d = 5 as the force density to a maximum of Λ = 7500 kN/m^3 shown in Figure 11(A). However, the maximum of force density dose not guarantee an improvement of the centerline effectiveness far away from the coolant hole. In the spanwise effectiveness (Fig. 11B), the reduced order model shows a tremendous cooling effect when the force density Λ is larger than Λ = 3000 kN/m^3. Interestingly, this spanwise effectiveness keeps on increasing with distance from the cooling hole. For example, at x/d = 6, the effectiveness increases from 0.07 to 0.45 as Λ varies from 0 to 7500 kN/m^3; at x/d = 15, it increases from 0.06 to 0.54 (~800% increase). Such increase confirms the active influence of plasma actuator in enhancing film cooling.

B. Concept_Two

Figure 12 plots the temperature distribution on the same planar location (x/d=4, 10, and 16) for four different geometric modifications and marks y-z plane temperature distribution at x/d = 4 for no actuation Λ = 0. At this distance the cold fluid lifts off in traditional design (a). As the distance increases at x/d =16 for design (a), the lift-off effect becomes aggravated. The situation worsens for (b) just beyond the bumper. However, for design (c) and (d), the cold jet bends (trips) for modest improvement of the cooling region on the work surface. In contrast, the influence of plasma induced electric force can be significant as seen in Figure 13 for Λ = 1500 kN/m^3. The temperature of the work surface reduced for all designs. For design (a) at x/d = 16, the lowest temperature 230 K on work surface is much cooler than in Figure 12 for the same design and location. In comparing designs b, c and d, it is evident that the cold jet attachment to the work surface increases from (b) to (c) to (d). It is thus essential to quantify the improvement in cooling performance.

Figure 14 plots the effect of plasma actuation on centerline effectiveness for four designs (a)-(d). Figure 14(A) shows the effect of geometric modifications (Λ = 0) of the cooling hole. The cooling performance of different hole shapes show that (c) and (d) have better centerline effectiveness at x/d = 4 (~40% increase) because the expansion of the jet reduces the momentum ratio increasing the cooling performance. Also the step at edge of (d) acts as a trip for the cold fluid inducing more attachment. Interestingly, bumper case (b) provides higher centerline effectiveness beyond x/d = 20 because the jump effect delays the cold fluid attached to the work surface. The centerline effectiveness of combinations of geometry modification and body force shown in Figure 14(B) increases by over 70%, 558%, 137%, and 164%, respectively, at x/d = 5 than in Figure 14(A) as the force density increases to Λ = 1500 kN/m^3 for designs (a)-(d).

Figure 15 shows the spanwise averaged effectiveness for four designs (a)-(d). Figure 15(A) shows the baseline design (a) has better spanwise effectiveness than that of (b) because the jump effect cause the counter-rotating vortex pair moving away from the wall. Design (c) and (d) have good improvement over 70% in spanwise effectiveness at x/d = 3 because the slot design reduces the momentum of cooling jet and gives more chances to cool the wall near the cooling hole. Figure 15(B) shows the plasma effect of designs (a)-(d) as force density increases to the maximum of Λ = 1500 kN/m^3. Evidently plasma actuation gives a very good improvement for designs (b)-(d). It is evident that the plasma actuation guarantees the flow attachment and the improvement of the heat transfer on the surface.

V. Conclusion

Two novel concepts are introduced for improving the film cooling. Concept one is using plasma actuator based on the phenomenological model and the reduced order model, and the results show a significant enhancement in streamwise and lateral cooling, improving the effectiveness by at least over 100%. Concept two using various hole shapes with plasma actuation shows a tremendous improvement of effectiveness for both streamwise and spanwise direction than without any geometric modification. In the near field region the reduced order model works better for improving cooling performance than the phenomenological model. The bumper design (b) did not appear as a good choice as compared to the configurations (c) and (d) to cool the surface near downstream of the hole. Application of plasma, however, remedies that shortfall. The hybrid DES and/or LES type turbulence model will possibly be better to capture such complex flow structures. Such effort will take much longer simulation time and may be another topic for a follow-on study. Realistic experimentation is underway to validate these designs. Plasma augmented design modified flow control ideas may become more beneficial for cases with badly separated jets at higher velocity ratio. This remains to be tested.

Acknowledgments

This work was partially supported by the AFOSR Grant Nos. FA9550-07-1-0131 and FA9550-09-1-0004 monitored by Dr. John Schmisseur.

References

[1]S. Roy, "Numerical Investigation of the Blade Cooling Effect by Multiple Jets Issuing at an angle," *Numerical Heat Transfer – Part A*, 38 (7), 2000, pp. 701-18.

[2]S. Kapadia, S. Roy and J. Heidmann, "First hybrid turbulence modeling for turbine blade cooling," *Journal of Thermophysics and Heat Transfer*, 18 (1), 2004, pp. 154-6.

[3]D.G. Hyams and J.H. Leylek, "A detailed analysis of film cooling physics: Part III— Streamwise injection with shaped holes," *Journal of Turbomachinery*, 122, 2000, pp. 122-32.

[4]S.V. Ekkad, S. Ou and R.B. Rivir, "Effect of jet pulsation and duty cycle on film cooling from a single jet on a leading edge model," *Journal of Turbomachinery*, 128, 2006, pp. 564-71.

[5]H. Kruse, "Measurements of film cooling effectiveness and heat transfer on a flat plate," *Heat and Mass Transfer in Rotating Machinery* (A86-24451 09-34), Washington, DC, Hemisphere Publishing Corp., 1984, pp. 451-461.

[6]A.K. Sinha, D.G. Bogard and M.E. Crawford, "Film-cooling effectiveness downstream of a single row of holes with variable density ratio," *Journal of Turbomachinery*, 113, 1991, pp. 442-9.

[7]R.S. Bunker, "A review of shaped hole turbine film-cooling technology," *Journal of Heat Transfer*, 127, 2005, pp. 441-453.

[8]J.H. Leylek and R.D. Zerkle, "Discrete-jet film cooling: A comparison of computational results with experiments," *Journal of Turbomachinery*, 111, 1994, pp. 358-68.

[9]R. Fearn and R.P. Weston, "Vorticity associated with a jet in a cross flow," *AIAA Journal*, 12, 1974, pp. 1666-1671.

[10]V.K. Garg and D.L. Rigby, "Heat Transfer on a Film-Cooled Blade - Effect of Hole Physics," *Int. J. Heat and Fluid Flow*, 20, 1999, pp.10-25.

[11]J.D. Heidmann, D.L. Rigby and A.A. Ameri, "A Three-Dimensional Coupled Internal/External Simulation of a Film-Cooled Turbine Vane," *Journal of Turbomachinery*, 122, 2000, pp. 348-359.

[12]Garg, V. K., "Heat Transfer on a Film-Cooled Rotating Blade," *Int. J. Heat and Fluid Flow*, 21, 2000, pp. 134-145.

[13]Lesieur, M., Comte, P., Lamballais, E., Métais, O., and Silvestrini, G., "Large-eddy simulations of shear flows," *J. Eng. Math.* , 32, 1997, pp. 195-215..

[14]Strelets, M., "Detached Eddy Simulation of Massively Separated Flows," AIAA 2001-0879, 2001.

[15]C.M. Ho and P. Huerre, "Perturbed Free Shear Layers," *Ann. Rev. Fluid Mech.*, 16, 1984, pp. 365-424.

[16]S. Roy and C.-C. Wang, "Bulk flow modification with horseshoe and serpentine plasma actuators," (Fast Track Communication) *Journal of Physics-D: Applied Physics*, 42, 2009.

[17]S. Roy, "Flow actuation using radio frequency in partially-ionized collisional plasmas," *Applied Physics Letters*, 86 (10) 101502, 2005.

[18]S. Roy and D. Gaitonde, "Force interaction of high pressure glow discharge with fluid flow for active separation control," *Physics of Plasmas*, 13 (2) 023503, 2006.

[19]A. Labergue, L. Leger, E. Moreau and G. Touchard, "Effect of a plasma actuator on an airflow along an inclined wall: P.I.V. and wall pressure measurements," *Journal of Electrostatics*, 63 (6-10), 2005, pp. 961-967.

[20]K.P. Singh and S. Roy, "Force approximation for a plasma actuator operating in atmospheric air," *Journal of Applied Physics*, 103, 013305, 2008.

[21]X. Z. Zhang and I. Hassan, "Film Cooling Effectiveness of an Advanced-Louver Cooling Scheme for Gas Turbine," J. Thermophys. Heat Transfer, 20 (4), 2006, pp. 754-64.

[22]J.D. Heidmann and S.D. Hunter, "Coarse Grid Modeling of Turbine Film Cooling flows using Volumetric Source Terms," ASME Paper 2001-GT-0138, 2001.
[23]A.A. Immarigeon, "Advanced Impingement/ Film-Cooling Schemes for High-Temperature Gas Turbine—Numerical Study," M.Sc. Thesis, Concordia Univ., Montreal, 2004.
[24]K. B. Mulugeta, and S. V. Patankar, "A Numerical Study of Discrete-Hole Film Cooling," ASME Paper 96-WA/HT-8, 1996.

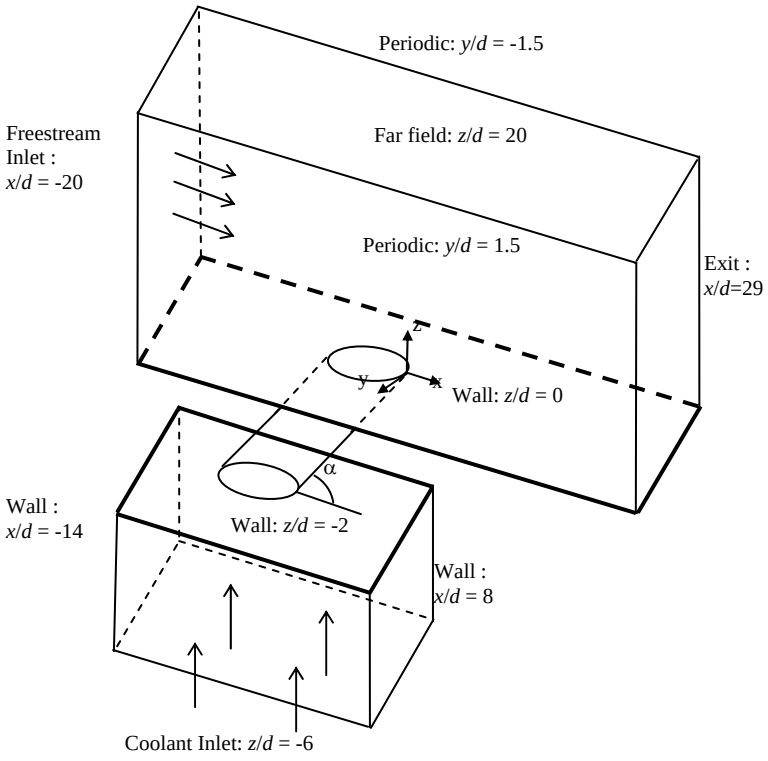

Figure 1. Schematic shows the film cooling flow. The geometry and boundary conditions are based on reported test setup.[6, 8]

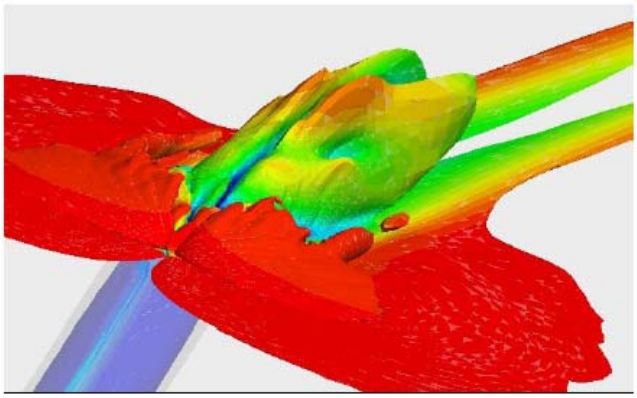

A) Counter rotating vortical structures at the jet exit plane is colored by the static temperature.

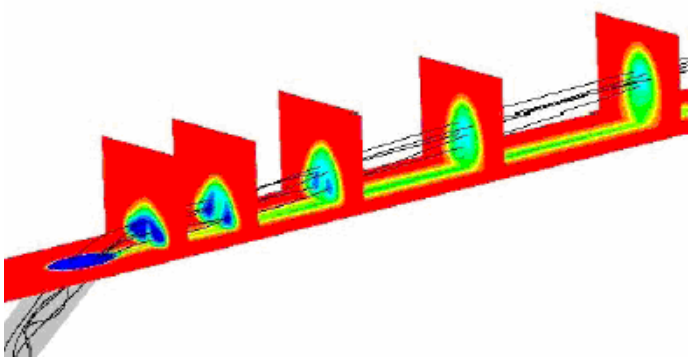

B) Diffusion of the cold jet into hot crossflow

Figure 2. DES simulation of film cooling shows the penetration of the cold jet is a three-dimensional process (From Kapadia *et al.*[2]).

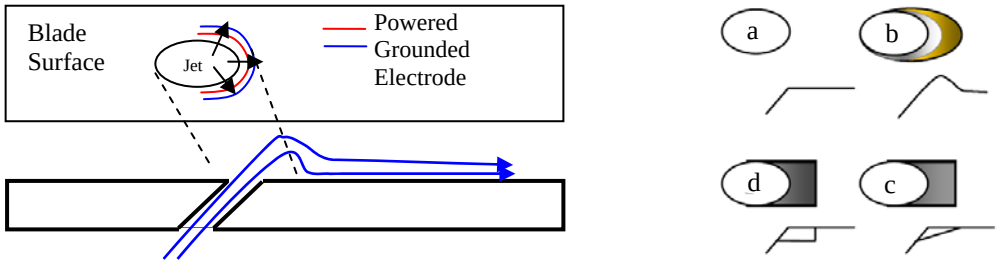

A) **B)**

Figure 3. Design modifications for improved cooling. A) Plasma actuator and B) Geometry modification.

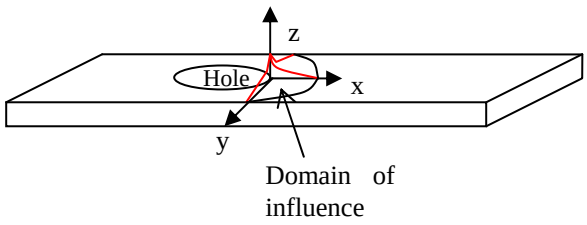

Figure 4. Force model used to approximate a plasma actuator.

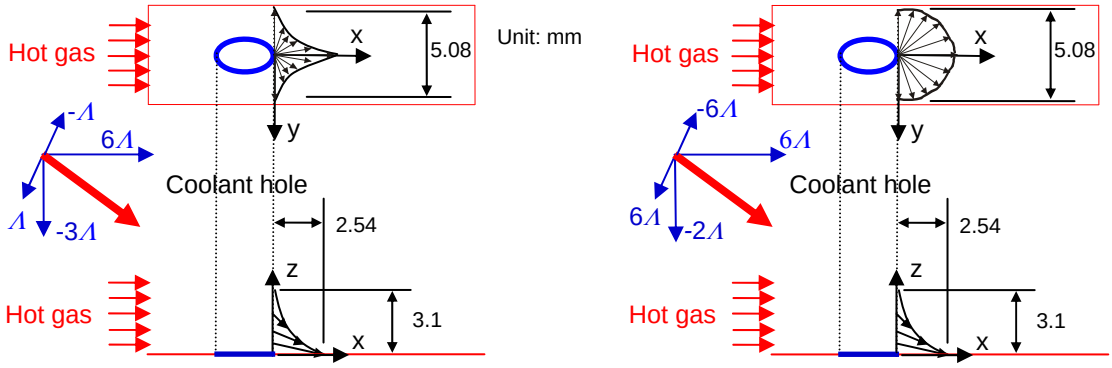

A) **B)**

Figure 5. Directional distribution of the force density for A) phenomenological model and B) reduced order model.

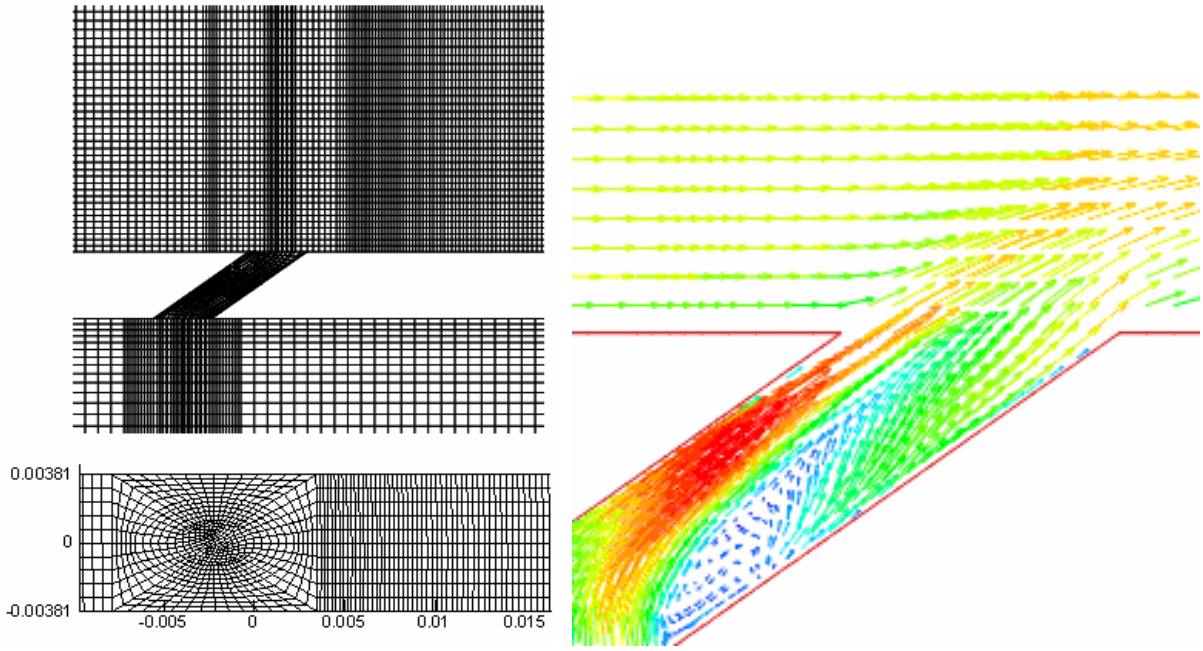

A) **B)**

Figure 6. A) Computational mesh details. B) Steady solution of the cooling pipe shows velocity vectors (red = 140 m/s, blue = 10 m/s) colored by fluid speed at the central (*y*=0) plane.

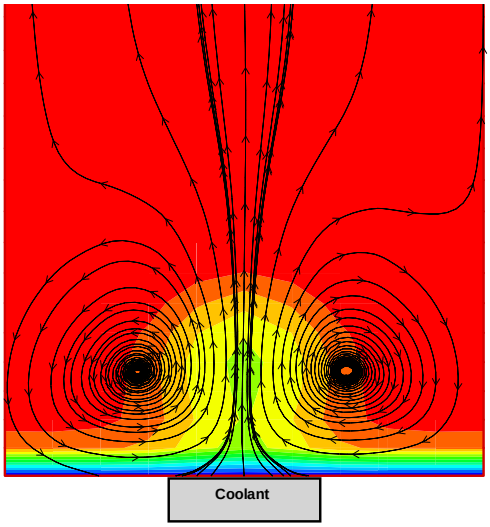

Figure 7. Stream trace at x/d = 5 over the velocity magnitude contour plot.

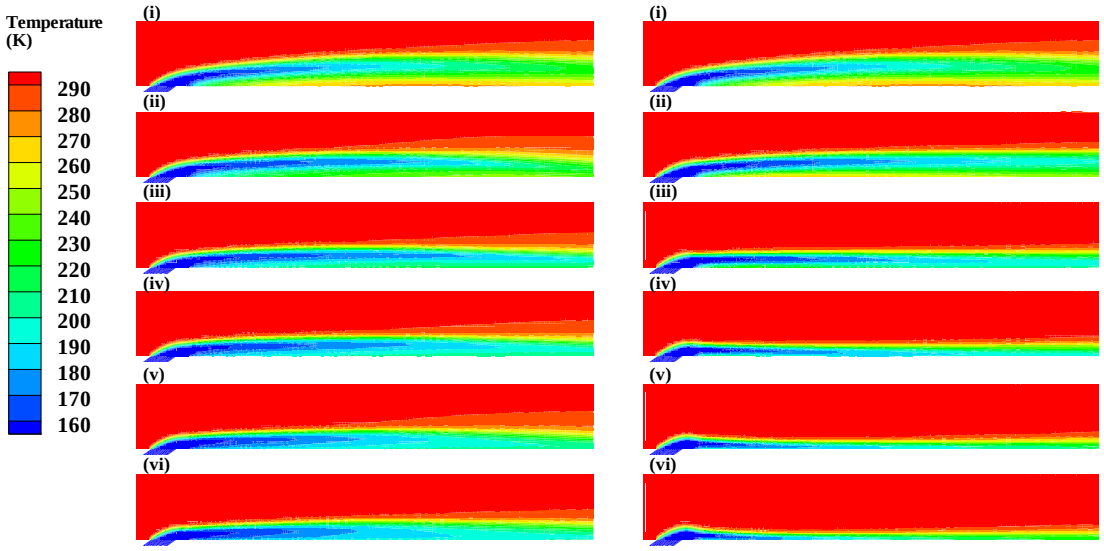

Figure 8. Temperature profile along the vertical plane at y = 0 plane for the amplitude of actuation force density Λ = (i) 0, (ii) 1500, (iii) 3000, (iv) 4500, (v) 6000, and (vi) 7500 kN/m^3 for A) phenomenological model and B) reduced order model.

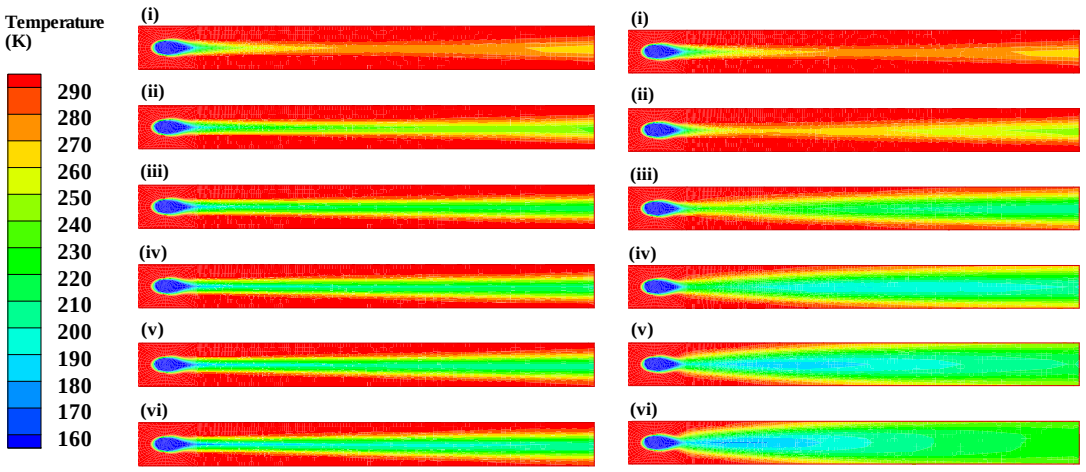

Figure 9. Temperature contour on the work surface (z=0) shows cooling flow attachment as actuation force density increases with the amplitude Λ = (i) 0, (ii) 1500, (iii) 3000, (iv) 4500, (v) 6000, and (vi) 7500 kN/m^3 for A) phenomenological model and B) reduced order model.

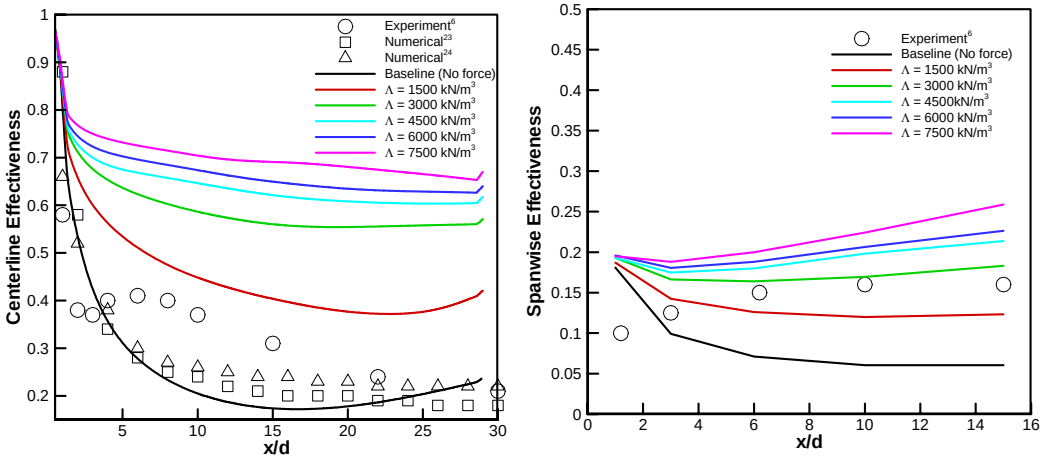

Figure 10. Effect of actuator force density based on *phenomenological model* shows significant increase in A) centerline effectiveness and B) spanwise effectiveness.

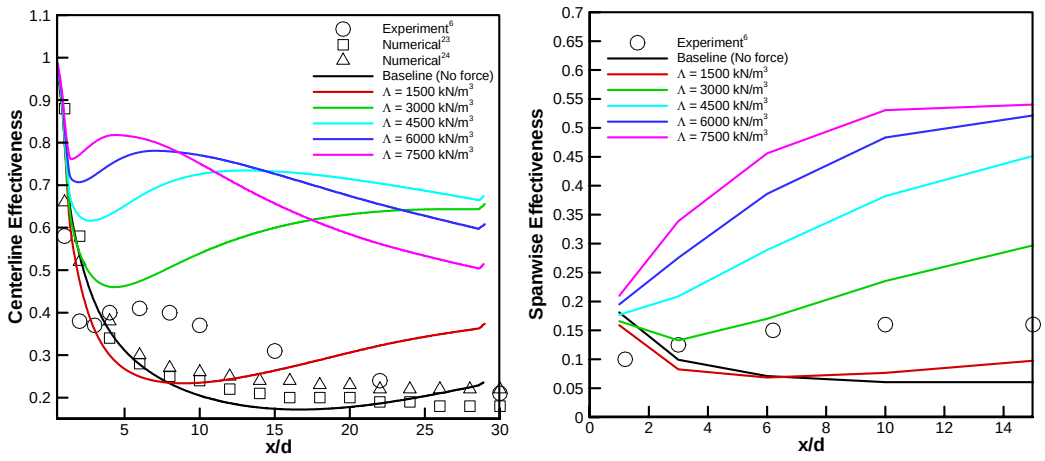

A) **B)**

Figure 11. Effect of actuator force density based on *reduced order model* shows significant increase in A) centerline effectiveness and B) spanwise effectiveness.

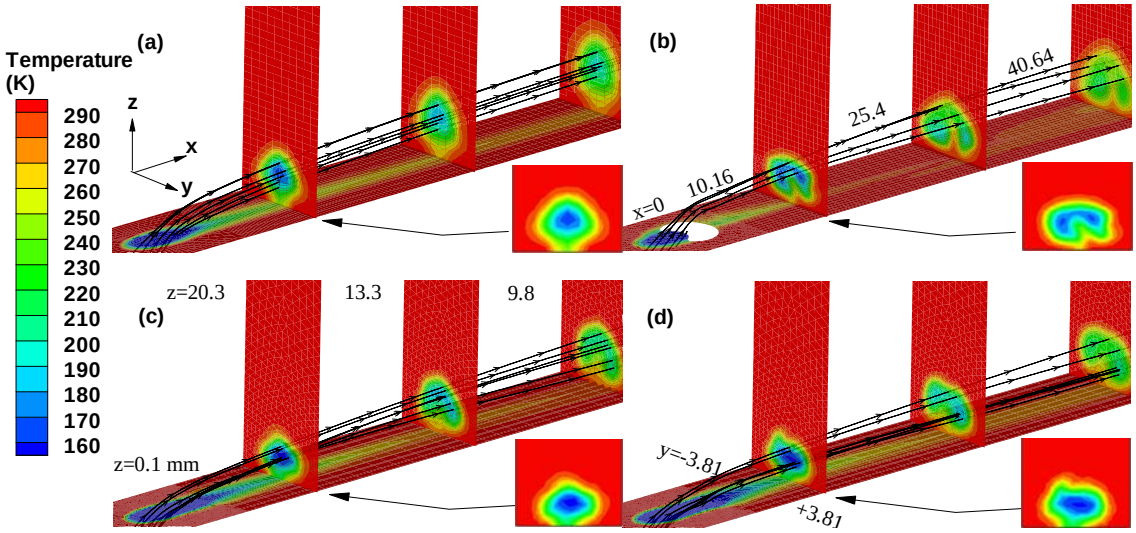

Figure 12. Temperature contours at spanwise plane (x/d=4, 10 and 16) for various designs (a)-(d).

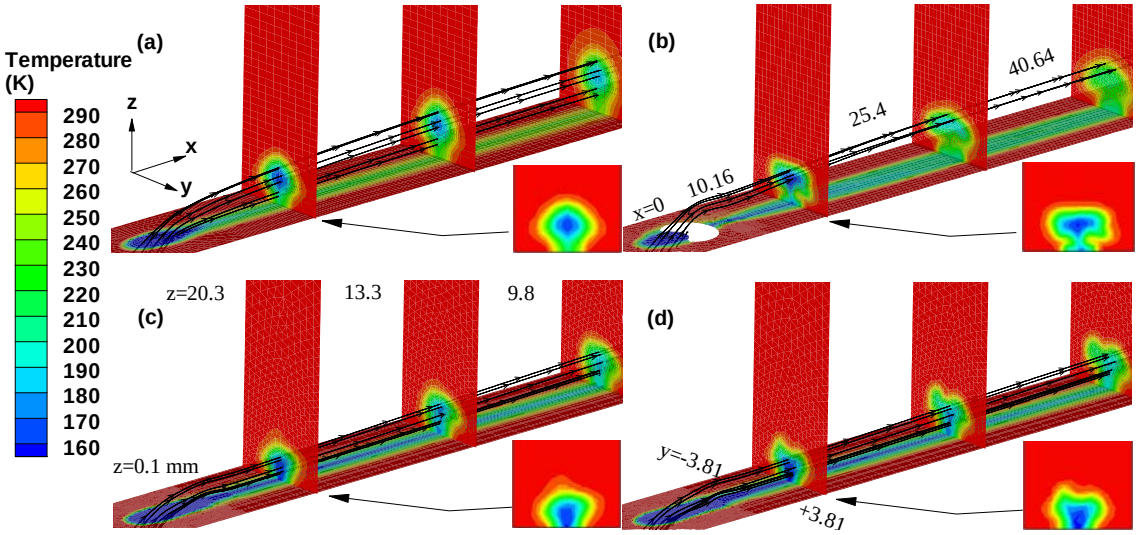

Figure 13. Temperature contours at spanwise plane (x/d=4, 10 and 16) for various designs (a)-(d) with actuation force density Λ=1500 kN/m^3

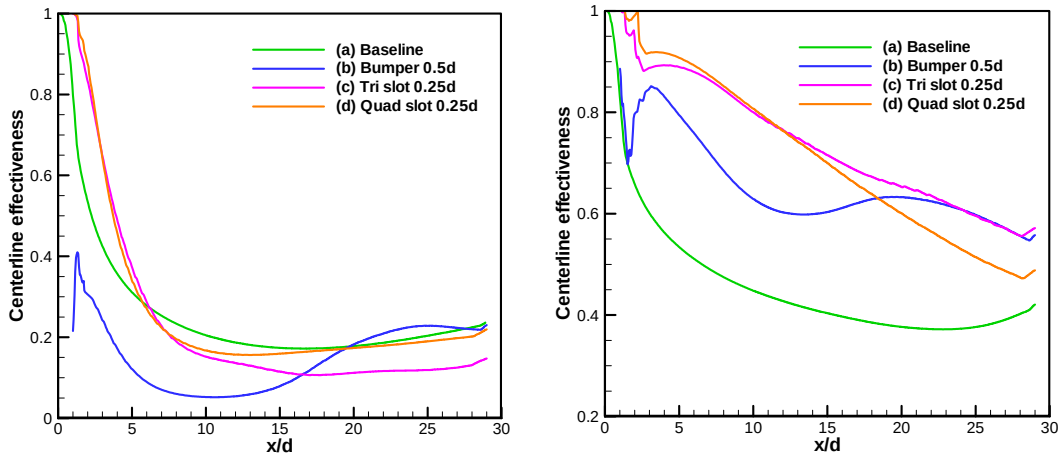

Figure 14. Effect of plasma actuation on centerline effectiveness for A) Λ = 0 and B) Λ = 1500 kN/m^3.

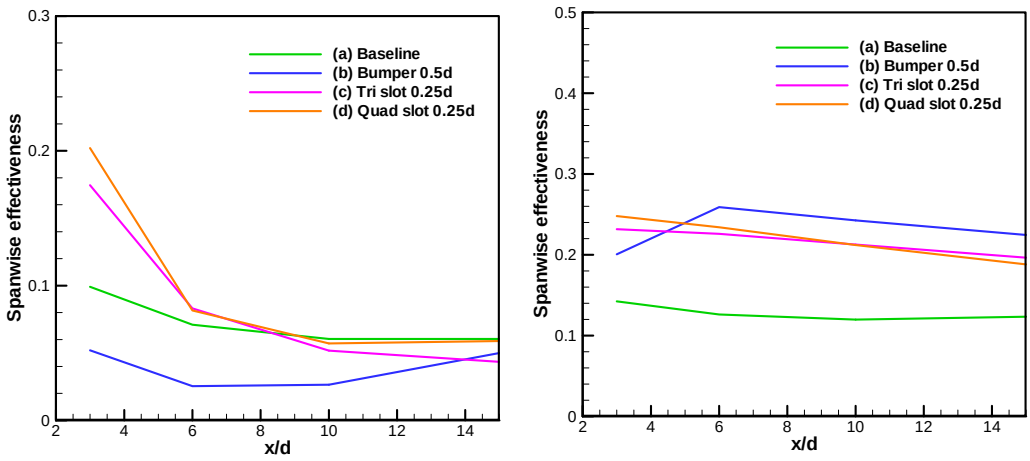

Figure 15. Effect of plasma actuation on spanwise effectiveness for A) Λ = 0 and B) Λ = 1500 kN/m^3.